A Survey of Electronic Properties in Bilayer Graphene

Arnab Adhikary, Bradley Guislain, Dongyang Yang, Jiabin Yu, and Yunhuan Xiao
Department of Physics and Astronomy,
University of British Columbia

(Dated: November 22, 2019)

Graphene has been a major point of interest in condensed matter physics since the late 1900s, when technology had advanced sufficiently to develop atomically thin layers of carbon, and theory had predicted that graphene would have novel electronic properties that could yield wide ranging applications in electronics. In this paper we will perform a basic theoretical analysis of the electronic band structure and properties of monolayer and bilayer graphene by constructing an effective Hamiltonian based on the tight binding model - we hope to demonstrate that the methods we have learned in PHYS 502 are sufficiently powerful to perform an analysis of graphene that reveals several of the interesting features that it is well known for. We will also provide a brief survey of some experimental methods used to probe the electron dynamics of graphene in the presence of electric and magnetic fields.

I. MONOLAYER GRAPHENE

We will begin our theoretical analysis of graphene by solving for the band structure in a non-interacting Hubbard model to obtain an approximate dispersion relation for monolayer graphene.

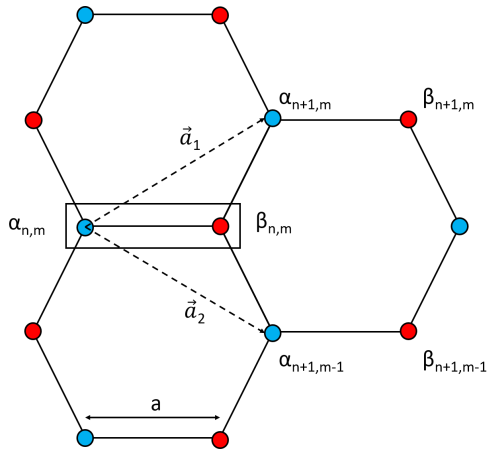

FIG. 1: The lattice structure of monolayer graphene. Lattice vectors are shown as dashed lines, and the minimal unit cell is illustrated as a rectangle surrounding the two inequivalent sites α and β.

A monolayer of graphene consists of single carbon atoms placed on a hexagonal "honeycomb" lattice - unit cells are constructed as shown in Fig. 1, with lattice sites at $\vec{R}_{nm}$ and lattice vectors:

$$\vec{a}_1 = a\left(\frac{3}{2}\hat{x} + \frac{\sqrt{3}}{2}\hat{y}\right)$$
$$\vec{a}_2 = a\left(\frac{3}{2}\hat{x} - \frac{\sqrt{3}}{2}\hat{y}\right)$$

So that:

$$R_{nm} = \vec{R}_0 + n\vec{a}_1 + m\vec{a}_2$$

The isolated carbon atoms have four valence electrons - though beyond the scope of this paper to show, the equilibrium electron configuration in graphene is well known and is illustrated in Fig. 2. The three hybridized sp^2 electrons are strongly bound, and the electrons that will be actively contributing to the band structure are those in p_z orbitals, giving effectively two valence electrons per unit cell.

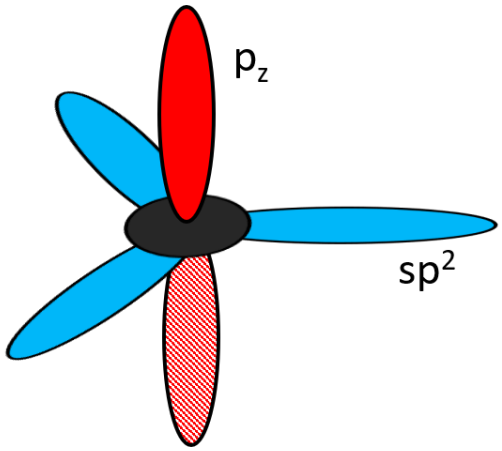

FIG. 2: An illustration of the valence orbital structure in graphene. Three electrons are tightly bound in hybridized sp^2 molecular orbitals, and the fourth is in an independent p_z orbital oriented out of the plane containing the honeycomb.

We will define γ_0 to be the positive hopping parameter (all of the p_z orbitals have a positive overlap) for nearest neighbour carbon atoms. Typical values of γ_0

obtained from experiment or first principles calculations range from 2.5-3 eV [1]. Assuming (quite fairly) that there is no difference in on-site energy between the two sites α and β , our Hamiltonian can now be written as follows:

$$\hat{H} = -\gamma_0 \sum_{n,m,\sigma} \beta^\dagger_{n,m,\sigma} \left(\alpha_{n+1,m,\sigma} + \alpha_{n+1,m-1,\sigma} + \alpha_{n,m,\sigma}\right) + h.c. \tag{1}$$

Where $\alpha^\dagger_{n,m,\sigma}$ creates an electron with spin σ at R_{nm} and $\beta^\dagger_{n,m,\sigma}$ creates an electron with spin σ at $R_{nm} + a\hat{x}$. Fourier transforming this Hamiltonian by transforming to a basis of Bloch eigenfunctions:

$$\begin{aligned} \alpha^\dagger_{\vec{k},\sigma} &= \sum_{n,m} \frac{e^{i\vec{k}\cdot\vec{R}_{nm}}}{\sqrt{N}} \alpha^\dagger_{n,m,\sigma} \\ \beta^\dagger_{\vec{k},\sigma} &= \sum_{n,m} \frac{e^{ik_x a} e^{i\vec{k}\cdot\vec{R}_{nm}}}{\sqrt{N}} \beta^\dagger_{n,m,\sigma} \end{aligned} \tag{2}$$

We obtain:

$$\begin{aligned} \hat{H} &= -\gamma_0 \sum_{\vec{k},\sigma} \beta^\dagger_{\vec{k},\sigma} \alpha_{\vec{k},\sigma} \left(e^{-ik_x a} + 2e^{\frac{ik_x a}{2}} \cos(k_y \tfrac{\sqrt{3}a}{2})\right) \\ &\quad + h.c. \\ &= -\gamma_0 \sum_{\vec{k},\sigma} f(\vec{k}) \beta^\dagger_{\vec{k},\sigma} \alpha_{\vec{k},\sigma} + f^*(\vec{k}) \alpha^\dagger_{\vec{k},\sigma} \beta_{\vec{k},\sigma} \end{aligned} \tag{3}$$

Where $f(\vec{k}) = e^{-ik_x a} + 2e^{\frac{ik_x a}{2}} \cos(k_y \frac{\sqrt{3}a}{2})$. It is then very simple to express our Hamiltonian as a matrix in the basis $\alpha^\dagger_{\vec{k},\sigma}, \beta^\dagger_{\vec{k},\sigma}$:

$$H = \begin{pmatrix} 0 & -\gamma_0 f^*(\vec{k}) \\ -\gamma_0 f(\vec{k}) & 0 \end{pmatrix} \tag{4}$$

Diagonalizing this Hamiltonian gives eigenbands:

$$\epsilon^\pm_{\vec{k}} = \pm\gamma_0 \sqrt{1 + 4\cos(k_x \tfrac{3a}{2}) \cos(k_y \tfrac{\sqrt{3}a}{2}) + 4\cos^2(k_y \tfrac{\sqrt{3}a}{2})} \tag{5}$$

Plots of this bandstructure are given in Figs. 3 and 4. Note that there are 6 points (2 unique, and 2 pairs at the edges of the Brillouin zone that are equivalent by symmetry) in the Brillouin zone where the energy in the conduction band meets the energy in the valence band at 0, giving graphene the structure of a **gapless semiconductor**. The density of states at these so called **Dirac points** is zero, which when combined with the zero bandgap gives graphene the properties of a semimetal at half-filling. Dirac points occur where:

$$\begin{aligned} &\epsilon_{\vec{k}} = 0 \\ &\implies 1 + 4\cos(k_x \tfrac{3a}{2}) \cos(k_y \tfrac{\sqrt{3}a}{2}) + 4\cos^2(k_y \tfrac{\sqrt{3}a}{2}) = 0 \end{aligned} \tag{6}$$

The two unique solutions appear at $k_x = 0$, $k_y = \pm\frac{4\pi}{3\sqrt{3}a}$, momenta which convention dictates we call $\vec{K}_\pm$. Since the Fermi level of pristine graphene at half-filling is at precisely these Dirac points, we're interested primarily in the dispersion in the vicinity of the $\vec{K}$ points. Taylor expanding the dispersion about the $\vec{K}_+$ point:

$$\begin{aligned} f(\vec{k}) &= e^{-ik_x a} + 2e^{\frac{ik_x a}{2}} \cos(k_y \tfrac{\sqrt{3}a}{2}) \\ \frac{\partial f(\vec{k})}{\partial k_x} &= -iae^{-ik_x a} + iae^{\frac{ik_x a}{2}} \cos(k_y \tfrac{\sqrt{3}a}{2}) \\ &\implies \frac{\partial f(\vec{k})}{\partial k_x}|_{\vec{K}_+} = -\frac{3a}{2}i \\ \frac{\partial f(\vec{k})}{\partial k_y} &= -\sqrt{3}ae^{\frac{ik_x a}{2}} \sin(k_y \tfrac{\sqrt{3}a}{2}) \\ &\implies \frac{\partial f(\vec{k})}{\partial k_y}|_{\vec{K}_+} = -\frac{3a}{2} \end{aligned} \tag{7}$$

With this gradient of $H_{\alpha\beta}$ at the origin, we can calculate an approximate dispersion at a point $\vec{k} - \vec{K} = v\vec{k}$ near the Dirac point:

$$\begin{aligned} H_{\alpha\beta} &\approx \nabla_{\vec{k}} H_{\alpha\beta}|_{\vec{k}_0} \cdot v\vec{k} \\ &= -\frac{3\gamma_0 a}{2}(ivk_x + vk_y) \\ \implies \epsilon^\pm_{\vec{k}} &= \pm\frac{3\gamma_0 a}{2}\sqrt{(vk_x)^2 + (vk_y)^2} \\ \implies \epsilon^\pm_{\vec{k}} &= \pm\frac{3\gamma_0 a}{2}|v\vec{k}| \end{aligned} \tag{8}$$

So sufficiently close to the Fermi level, we have a conical dispersion that is linear in $|v\vec{k}|$ This conical bandstructure approximation near the two "valleys" as they are often called in condensed matter physics will be very useful in subsequent sections, making several problems involving a cumbersome 4-band Hamiltonian analytically tractable.

These **Dirac cones** are also interesting in their own right - a linear dispersion is exactly what the Dirac equation predicts for massless or ultrarelativistic fermions, as opposed to the quadratic dispersion we typically expect for an electron propagating in free space (or bound near the Fermi level in a more conventional lattice, like the 1D chain for example). As you might expect, this leads to some fascinating properties, several of which will be discussed in subsequent sections. Of course, right now you

may be very skeptical of the claims we have made here, and rightly so, since our model is extremely simple - it turns out, however, that it has been shown both mathematically [2] and in experiment [3] that graphene does in fact exhibit a zero bandgap and conical dispersion near the Fermi level, just as a simple tight binding model has predicted here in our analysis.

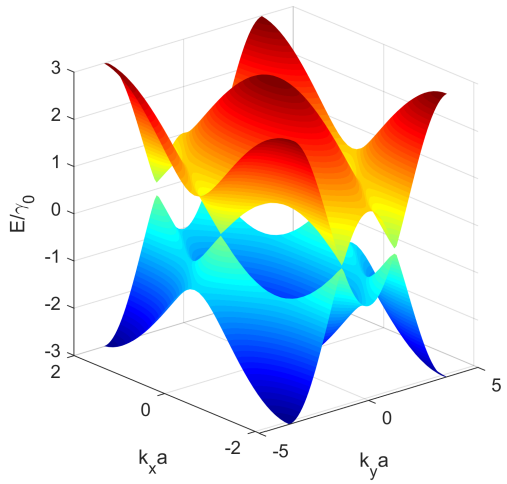

FIG. 3: The band structure of monolayer graphene in the tight binding approximation, plotted within the first Brillouin zone.

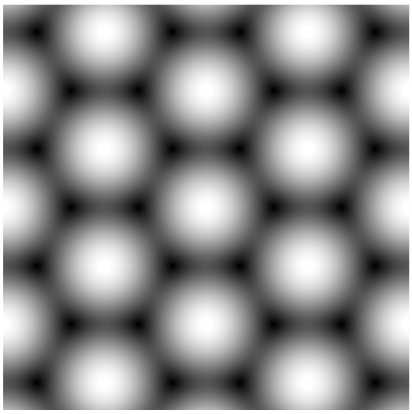

FIG. 4: Several periods of the band structure of the (+) band plotted as a heat map in k_x and k_y. Since the reciprocal lattice for a honeycomb lattice is also a honeycomb, the energy levels are "honeycomb periodic", making them look something like an STM image of graphene when plotted like this - we all thought this was very neat.

II. BILAYER GRAPHENE

Now that we have developed a basic picture of the band structure and electronic properties of a single layer of graphene, an obvious question to ask is what happens in structures of multiple stacked layers of carbon atoms in a honeycomb lattice. The simplest of these is a layer of two graphene sheets, depicted in Fig.5. Intuition tells us that the lowest energy configuration of the nuclei should have the layers staggered with respect to one another to minimize the Coulomb repulsion between layers - Ab-initio calculations [4] have demonstrated that this is true, and that the most stable configuration of bilayer graphene is this so called "AB stacked" or "Bernal stacked" configuration.

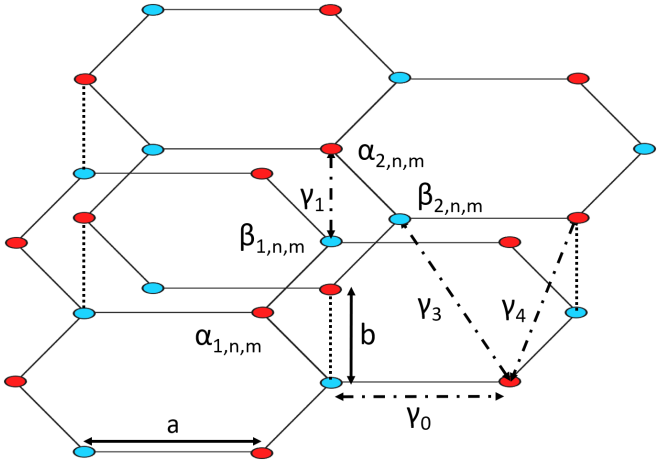

FIG. 5: An illustration of the bilayer graphene lattice with AB stacking. The unit cell is labelled with greek letters, and the relevant hopping parameters are shown as a dashed line.

We can construct bilayer graphene on a lattice that is identical to the monolayer graphene lattice - the difference now being that the unit cell contains four atoms. Atoms α_1 and β_1 are configured precisely as the atoms α and β were in the monolayer problem, atoms α_2 sit a distance b directly above atoms β_1, and atoms β_2 sit a distance b directly above the vacant center of the honeycomb structures in the monolayer. We will adopt the standard convention in the literature for labelling the hopping parameters, and provide their known values from Raman scattering experiments [5]:

- $\gamma_0 \approx 2.9eV$ - Between (α_1, β_1) and (α_2, β_2)
- $\gamma_1 \approx 0.30eV$ - Between (β_1, α_2)
- $\gamma_3 \approx 0.10eV$ - Between (α_1, β_2)
- $\gamma_4 \approx 0.12eV$ - Between (α_1, α_2) and (β_1, β_2)

At first you might be shocked (as were we) that at no point in this paper will a γ_2 appear - this is because when discussing allotropes of carbon, γ_2 and γ_5 are reserved for the two layer hopping from one atom to its equivalent in AB stacked graphite.

All of these parameters carry a positive sign, and in writing the Hamiltonian it will be important to note that the integrals responsible for interlayer hopping are overlap integrals between p_z lobes of opposite phase, which will introduce a negative sign. We will allow for some degree of *interlayer asymmetry* in this model - that is, the on-site energy will be different for the top and bottom layers by some amount 2δ. There's not any particular reason for this to be the case for pristine bilayer graphene in the absence of any doping or external field, but it is a valuable addition to this analysis to be able to visualize what the effect on the band structure is for nonzero δ, as we will introduce effects in subsequent sections that cause this to be the case.

The Hamiltonian can now be written:

$$\begin{aligned}
H =& H_{in-plane,1} + H_{in-plane,2} \\
&+\delta \sum_{n,m,\sigma} \Big(\alpha^\dagger_{1,n,m,\sigma}\alpha_{1,n,m,\sigma} + \beta^\dagger_{1,n,m,\sigma}\beta_{1,n,m,\sigma} \\
&\quad -\alpha^\dagger_{2,n,m,\sigma}\alpha_{2,n,m,\sigma} - \beta^\dagger_{2,n,m,\sigma}\beta_{2,n,m,\sigma} \Big) \\
&+\gamma_1 \sum_{n,m,\sigma} \beta^\dagger_{1,n,m,\sigma}\alpha_{2,n,m,\sigma} + h.c. \\
&+\gamma_3 \sum_{n,m,\sigma} \alpha^\dagger_{1,n,m,\sigma} \left(\beta_{2,n,m,\sigma} + \beta_{2,n-1,m,\sigma} + \beta_{2,n,m+1,\sigma}\right) + h.c. \\
&+\gamma_4 \sum_{n,m,\sigma} \Big(\alpha^\dagger_{1,n,m,\sigma} \left(\alpha_{2,n,m,\sigma} + \alpha_{2,n-1,m,\sigma} + \alpha_{2,n-1,m-1,\sigma}\right) \\
&\quad + \beta^\dagger_{1,n,m,\sigma} \left(\beta_{2,n,m,\sigma} + \beta_{2,n+1,m-1,\sigma} + \beta_{2,n+1,m,\sigma}\right) \Big) + h.c.
\end{aligned}$$

Where $H_{in-plane,1}$ is the Hamiltonian as written for the monolayer with hopping parameter γ_0, and $H_{in-plane,2}$ is the same, but for the upper layer in the basis $\alpha_2^\dagger$, $\beta_2^\dagger$.

Fourier transforming into a basis of Bloch eigenfunctions is deceptively simple in the bilayer case. We can note that there are only two distinct patterns in the hopping Hamiltonians - the same sort of tetragonal pattern that appeared in the monolayer appears, as well as an inverted tetragonal pattern that will result in a complex conjugate of the same function of $\vec{k}$ appearing in the Hamiltonian. The vertical out of plane hopping introduces only a constant to the Hamiltonian, since the two sites are not separated at all as far as the lattice is concerned. In matrix form, with a basis $(\alpha_1, \beta_1, \alpha_2, \beta_2)$, the Hamiltonian becomes:

$$H = \begin{pmatrix} \delta & -\gamma_0 f(\vec{k}) & \gamma_4 f(\vec{k}) & \gamma_3 f^*(\vec{k}) \\ -\gamma_0 f^*(\vec{k}) & \delta & \gamma_1 & \gamma_4 f(\vec{k}) \\ \gamma_4 f^*(\vec{k}) & \gamma_1 & -\delta & -\gamma_0 f(\vec{k}) \\ \gamma_3 f(\vec{k}) & \gamma_4 f^*(\vec{k}) & -\gamma_0 f^*(\vec{k}) & -\delta \end{pmatrix} \quad (9)$$

Where, as we recall from the monolayer analysis,

$$f(\vec{k}) = e^{-ik_x a} + 2e^{\frac{ik_x a}{2}} \cos(k_y \frac{\sqrt{3}a}{2})$$

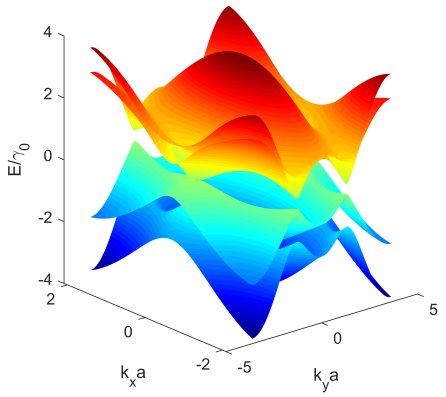

FIG. 6: The band structure of bilayer graphene in the first Brillouin zone. Parameters used for this figure: $\gamma_1 = 0.8\gamma_0$, $\gamma_3 = 0.2\gamma_0$, $\gamma_4 = 0.2\gamma_0$, $\delta = 0$

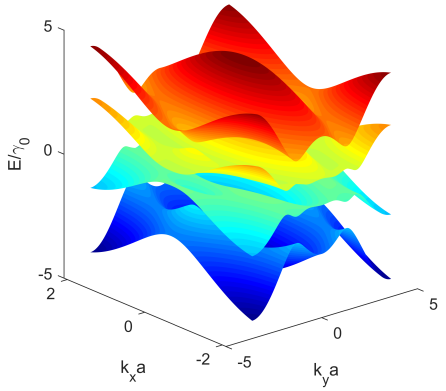

FIG. 7: The band structure of bilayer graphene in the first Brillouin zone. Parameters used for this figure: $\gamma_1 = 0.8\gamma_0$, $\gamma_3 = 0.2\gamma_0$, $\gamma_4 = 0.2\gamma_0$, $\delta = \gamma_0$

In principle, this Hamiltonian could be analytically diagonalized for the eigenbands. This would be very cumbersome and not especially educational. The system is perfectly amenable to being numerically diagonalized in

MATLAB however, which we have done to Figs. 6 and 7. To produce these plots, we've chosen an exaggerated and unrealistic set of hopping parameters in order to illustrate the features of the band structure clearly - in reality the lowest and highest energy bands are nearly degenerate with the two center bands due to the interlayer hopping being very weak in comparison to γ_0.
If you're interested in reproducing these figures or exploring the band structure for different values of the parameters in the Hamiltonian, source code is provided in **Appendix B**.

III. EFFECTIVE HAMILTONIAN OF BILAYER GRAPHENE

A. Effective four band Hamiltonian near K and $K^{'}$

A rigorous Hamiltonian for bilayer graphene has been derived in the previous section based on the tight-binding model, which can be used to describe the dispersion for any wavevector k in the Brillouin Zone. However, we are more interested in low energy properties which are dominated by the band structure near the two valleys. Equation (9) describing nearest neighbor hopping can be expanded near K and $K^{'}$ points to give us:

$$f(k_x, k_y) \approx -\sqrt{3}a(\tau k_x - ik_y)/2 \tag{10}$$

in which k_x, k_y are in-plane momenta measured relative to the valley in question. Here we introduce the notation τ for the *valley degree of freedom*, $\tau = \pm 1$. $\tau = +1$ represents valley $K = (4\pi/3a, 0)$, while $\tau = -1$ refers to $K^{'} = (-4\pi/3a, 0)$. Using this, we can write an approximate bilayer Hamiltonian:

$$H_b = \begin{pmatrix} \delta & v_0(\tau k_x - ik_y) & -v_4(\tau k_x - ik_y) & v_3(\tau k_x + ik_y) \\ v_0(\tau k_x + ik_y) & \delta & \gamma_1 & -v_4(\tau k_x - ik_y) \\ -v_4(\tau k_x + ik_y) & \gamma_1 & -\delta & v_0(\tau k_x - ik_y) \\ v_3(\tau k_x - ik_y) & -v_4(\tau k_x + ik_y) & v_0(\tau k_x + ik_y) & -\delta \end{pmatrix} \tag{11}$$

Where we introduce inter-layer coupling constants:

$$v_0 = \frac{\sqrt{3}a\gamma_0}{2} \qquad v_3 = \frac{\sqrt{3}a\gamma_3}{2} \qquad v_4 = \frac{\sqrt{3}a\gamma_4}{2} \tag{12}$$

Knowing how the hopping integrals compare in real AB-stacked bilayer graphene will allow us to simplify the Hamiltonian even further. As was stated in section 1, for Bernal stacked bilayer graphene we have:

$$\gamma_0 \gg \gamma_1 > \gamma_3, \gamma_4 \tag{13}$$

This can be easily understood by noting that the interlayer distance a between carbon atoms is larger than the intralayer separation b in the most stable configuration of bilayer graphene [3], and γ_1 will be significantly larger than the other interlayer hopping parameters due to a much larger overlap between the p_z orbitals belonging to atoms that are directly opposite one another. So the interlayer coupling terms $v_3(\tau k_x \pm ik_y)$ and $v_3(\tau k_x \pm ik_y)$ in the off-diagonal part of the bilayer Hamiltonian are at least one order of a smaller than γ_1 due to the fact that k_x and k_y are small deviations from the K point. In this case, the bilayer graphene Hamiltonian can be further reduced to an even more simplified form, which is known as the effective four band Hamiltonian around the two valleys [6].

$$H_{eb} = \begin{pmatrix} \delta & v_0(\tau k_x - ik_y) & 0 & 0 \\ v_0(\tau k_x + ik_y) & \delta & \gamma_1 & 0 \\ 0 & \gamma_1 & -\delta & v_0(\tau k_x - ik_y) \\ 0 & 0 & v_0(\tau k_x + ik_y) & -\delta \end{pmatrix} \tag{14}$$

B. Effective two band Hamiltonian

In the vicinity of the two valleys, the effective four band Hamiltonian derived in subsection A can be easily diagonalized by hand. Doing this reveals that the two outer bands are highly localised in a superposition of the α_2 and β_1 orbitals, often called a dimer site in the literature. The two inner bands then correspond to atoms localized at α_1 and β_2 . Note that these states are entirely decoupled from the dimer sites under our effective 4 site Hamiltonian - the last two elements in the first row as well as the first two elements in the last row are zero. If the carrier density is low enough, the two outer bands make no contribution to the electronic properties of the system. For zero external field ($\delta = 0$) and small on-site energy difference, the dispersion for all four bands is given as follows:

$$E_1 = \pm\frac{\gamma_1}{2}\left(\sqrt{1 + \frac{4v_0k^2}{\gamma_1^2}} - 1\right) \tag{15}$$

$$E_2 = \pm\frac{\gamma_1}{2}\left(\sqrt{1 + \frac{4v_0k^2}{\gamma_1^2}} + 1\right) \tag{16}$$

Where E_1 is the dispersion for the inner two bands and E_2 for the outer bands, which can be easily seen by setting $k = 0$.

For the inner bands:

$$\begin{aligned} k \ll \gamma_1/v_0 \implies \qquad & E_1 \approx \pm\frac{\hbar^2k^2}{2m^*}, \qquad m^* = \frac{\hbar^2\gamma_1}{2v_0^2} \\ k \gg \gamma_1/v_0 \implies \qquad & E_1 \approx \pm v_f\hbar k \qquad v_f = \frac{v_0}{\hbar} \end{aligned} \tag{17}$$

Implying that at low carrier density, the inner bands have a dispersion corresponding to that of a massive fermion with mass m^*. The Fermi level of a 2D electron gas with

density N is given by:

$$k_F = (\pi N)^{1/2} \tag{18}$$

Where we have already taken spin and valley degeneracy into account. $k \ll \gamma_1/v_0$ corresponds to a density $N^* = 8.72 \times 10^{12} cm^{-2}$ [7]. The carrier density N^* is relatively high in experiments even with electrical doping, so the conditions we have assumed are justified in most natural situations. We can make a simple estimation to justify this as well - a typical capacitance for $300nm$ thick silicon dioxide is roughly $10^{-10} F/cm^2$, which means it can host an electron density of $10^{12} cm^{-2}$ under $100V$, which is usually comparable to or beyond the breakdown voltage of a typical device used in experiments, so it is fair to assume that the two high energy bands can be neglected when exploring low energy properties.

Combining these approximations, a much more efficient way to describe the bilayer Hamiltonian at low energy is to eliminate the dimer site components completely, reducing our Hilbert space to the space spanned by non-dimer sites α_1 and β_2. The basic idea is to project the effective four band Hamiltonian onto this non-dimer site basis. If we ignore the on-site energy difference and v_3 ,v_4 contributions, we get an effective two band Hamiltonian describing the two center bands at a K valley. The detailed procedure is just a matter of linear algebra, and is expanded upon in Appendix A.[8]

$$H_{eff} = -\frac{\hbar^2}{2m}\begin{pmatrix} 0 & (\pi^\dagger)^2 \\ (\pi)^2 & 0 \end{pmatrix} + \delta \begin{pmatrix} 1 & 0 \\ 0 & -1 \end{pmatrix} \quad \pi = k_x + ik_y \tag{19}$$

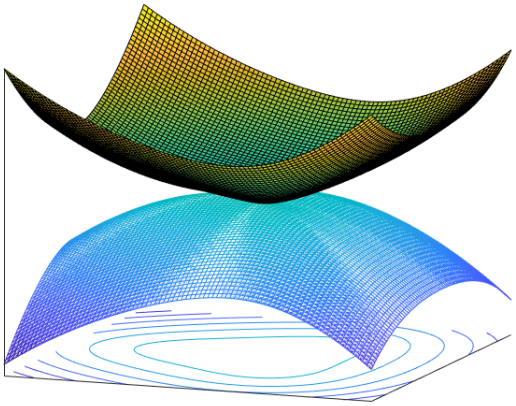

FIG. 8: The effect of the warping term H_w will be to distort the circular iso-energy lines, reducing them to a three-fold triangular symmetry. The strength of the warping term has been exaggerated for the purpose of illustration.

It should be noted that the effective two band Hamiltonian derived above is based on the simplest four band Hamiltonian, which can be viewed as a zero order approximation. If we take the inter-layer coupling v_3 into account and use the same procedure, there will be a first order correction near the K valley,

$$H_w = v_3 \begin{pmatrix} 0 & \pi \\ \pi^\dagger & 0 \end{pmatrix} \tag{20}$$

The effect of this Hamiltonian correction is a trigonal warping of the bandstructure's iso-energy lines as shown in Fig. 8.

C. General solution of the Two Band Effective Hamiltonian

In this subsection, we are going to discuss the general solutions of biased bilayer graphene based on the effective two band Hamiltonian. At the K valley,

$$\begin{aligned} H_{eff} &= \begin{pmatrix} \delta & -\frac{v_0^2}{\gamma_1} k^2 e^{-i2\phi_k} \\ -\frac{v_0^2}{\gamma_1} k^2 e^{i2\phi_k} & -\delta \end{pmatrix} \\ k &= \sqrt{k_x^2 + k_y^2} \\ \phi_k &= \tan(k_y/k_x) \end{aligned} \tag{21}$$

The general solution of this 2×2 Hamiltonian is $E = \pm\sqrt{\delta^2 + \frac{v_0^4}{\gamma_1^2} k^4}$ with corresponding eigenstates in the conduction band and valence band [7]:

$$|c,k\rangle = \begin{pmatrix} \cos(\frac{\theta_k}{2}) \\ \sin(\frac{\theta_k}{2}) e^{2i\phi_k} \end{pmatrix} \qquad |v,k\rangle = \begin{pmatrix} \sin(\frac{\theta_k}{2}) e^{-2i\phi_k} \\ \cos(\frac{\theta_k}{2}) \end{pmatrix} \tag{22}$$

where $\cos\theta_k = \frac{\delta}{\sqrt{\delta^2 + \frac{v_0^4}{\gamma_1^2} k^4}}$ Because we're operating in the basis (α_1, β_2), each component in the wave function represents the probability amplitude for an electron to be found in the top layer or bottom layer of bilayer graphene, i.e. one conduction band electron with a wave vector (k_x, k_y) could be found in the top layer with a probability $\cos^2(\frac{\theta_k}{2})$.

IV. TUNABILITY OF BILAYER GRAPHENE'S BANDGAP

Although graphene's characteristic zero bandgap has limited its application for electronics, it has been proven possible to open a bandgap in bilayer graphene. Successful experimental attempts include one side chemical doping [9, 10], single electrical gate tuning [11, 12] and dual gate tuning [13]. Notably, employing a dual external gate configuration, a controllable doping can be achieved with a widely tunable bandgap can be demonstrated.

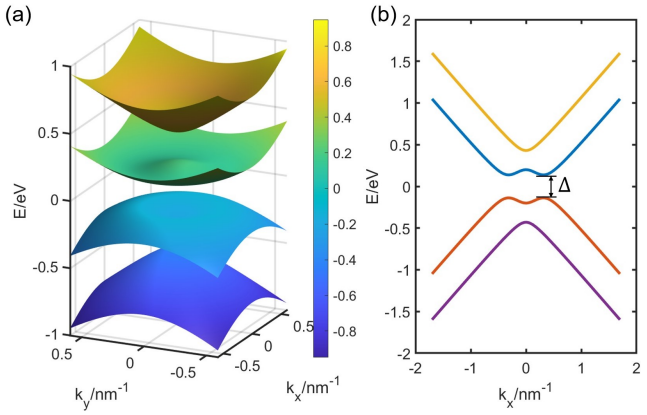

FIG. 9: Band diagram of bilayer graphene with $\delta \neq 0$. (a) The "Mexican-hat" shape band diagram. (b) A bandgap Δ opens up.

A. Band structure with interlayer asymmetry

Pristine bilayer graphene, similar to its monolayer counterpart, is gapless with lower energy bands touching each other at K and K'.. However, either asymmetric doping or a vertically applied electric field can lead to an asymmetry between the top and bottom layers, since there is now a gradient in potential between the top and bottom layers, which can give a nonzero relative on-site energy 2δ. We can obtain the band structure in this case by solving exactly the four band effective Hamiltonian Eq.14. Writing the energies as $E = \pm E_n$, $n = 1, 2$, we obtain,

$$E_n^2 = \frac{\gamma_1^2}{2} + \delta^2 + v_0^2 k^2 + (-1)^n \sqrt{\Omega} \tag{23}$$

$$\Omega = \frac{1}{4}\gamma_1^4 + v_0^2 k^2 (\gamma_1^2 + 4\delta^2) \tag{24}$$

where $\tau = \pm 1$ denotes the K_τ valley, $k = \sqrt{k_x^2 + k_y^2}$ and $\phi_k = \arctan(k_y/k_x)$. Lower energy bands $\pm E_1$ represent the interlayer coupling between non-dimer sites α_1, β_2. Higher energy bands $\pm E_2$ are related with the coupling γ_1 between the orbitals on the dimer sites α_2, β_1. The asymmetry 2δ would yield a band diagram like the one shown in Fig. 9(a), in which a "Mexican-hat" shape appears for the lower bands. Apart from the change in band shape, a bandgap Δ opens up,

$$\Delta = \frac{|2\delta|\gamma_1}{\sqrt{\gamma_1^2 + 4\delta^2}}. \tag{25}$$

It's worth noticing that for large interlayer asymmetry values $|2\delta| \gg \gamma_1$, the bandgap goes to the limit γ_1, whose value is typically around a few hundred meV. The opened bandgap is illustrated in Fig. 9(b).

B. Self-consistent tight-binding

As mentioned in the previous subsection, an external applied potential could be an effective tool for controlling the interlayer asymmetry 2δ. However, apart from this contribution, changing the vertically applied external field will also induce doping in graphene devices, changing the electron density N. This is called a screening effect, as with extra charges accumulating on both graphene layers, the electrons on them will not only feel the field caused by the gates, but also a field produced by the difference in charge between layers. Because of this effect, the interlayer on-site energy asymmetry as well as the bandgap will be altered and take a somewhat more complicated form when expressed as a function of gate voltage than what we would expect without any screening considered. In this section, making use of the effective Hamiltonian derived previously, we will investigate the functional dependence of the bandgap in bilayer graphene to an applied external field.

Based on the general solutions of the effective two band Hamiltonian, intuitively, the number of electrons per unit area could be directly computed by multiplying the density of states at a value of k with the states occupation probability[14], to get

$$N = g \int \Psi^\dagger(k)\Psi(k) \frac{k dk d\theta}{(2\pi)^2} \tag{26}$$

In bilayer graphene, we have good quantum numbers τ and σ corresponding to spin and valley degrees of freedom, making the degeneracy factor for a given k, $g = 4$. For the upper layer, the electronic wave function in the conduction band is $|c_1, k\rangle = \cos\frac{\theta_k}{2}$. According to this solution, conduction band electron density in top layer is given by:

$$\begin{aligned} N_t^{cb} =& \frac{1}{\pi}\int_0^{k_F} k dk + \frac{1}{\pi}\int_0^{k_F} \cos\theta_k k dk \\ =& \frac{N}{2} + \frac{N_c\delta}{2\gamma_1}\ln\left(\frac{N\gamma_1}{N_c\delta} + \sqrt{1 + \left(\frac{N\gamma_1}{N_c\delta}\right)^2}\right) \\ N_c =& \frac{\gamma_1^2}{\pi v_0^2} \end{aligned} \tag{27}$$

Unlike the conduction band, the valence band is normally fully filled in the ground state. In order to compute an electron density contribution from the valence band, we can note that there is a wave vector cut off k_c beyond which effective two band Hamiltonian fails. This is exactly the point where parabolic dispersion and linear dispersion cross with each other at $k_c = \gamma_1/v_0$, as discussed in section 3A. If we assume that we can only transfer electrons across layers that do not break the assumptions that made our two band Hamiltonian valid, the top layer

valence band electron density reads:

$$\begin{aligned} N_t^{vb} =& \frac{1}{\pi}\int_0^{k_c} kdk - \frac{1}{\pi}\int_0^{k_c} \cos\theta_k kdk \\ =& \frac{N_c}{2} - \frac{N_c\delta}{\gamma_1}\ln\left(\frac{\gamma_1}{\delta} + \sqrt{1+(\frac{\gamma_1}{\delta})^2}\right) \end{aligned} \tag{28}$$

Similarly, we get bottom layer conduction band and valence band electron density.

$$\begin{aligned} N_b^{cb} &= \frac{N}{2} - \frac{N_c\delta}{2\gamma_1}\ln\left(\frac{N\gamma_1}{N_c\delta} + \sqrt{1+(\frac{N\gamma_1}{N_c\delta})^2}\right) \\ N_b^{vb} &= \frac{N_c}{2} + \frac{N_c\delta}{\gamma_1}\ln\left(\frac{\gamma_1}{\delta} + \sqrt{1+(\frac{\gamma_1}{\delta})^2}\right) \end{aligned} \tag{29}$$

We will only examine pristine, charge neutral graphene with $N = 0$. In the ground state, we then have zero electron density in the conduction band, and the total valence band electron density is $N_c = k_c^2/\pi$, where we are assuming the only electrons available to interact with the external field are those near the Fermi level in the vicinity of k_c. In an external field, the electrons will redistribute along the interlayer axis. Forcing a portion of the electrons n^* from the lower layer's valence band to the upper layer's valence band in this way creates a nonzero net charge for the individual layers. In this case, if we denote the externally applied electric displacement as D_{ext}, the elementary charge to be e, the spacing between the two graphene layers to be b as before, and the dielectric constant for the space between the layers to be ϵ_{BLG}, then the difference in potential energy between the two layers satisfies the following equation:

$$2\delta = \frac{D_{ext}ed}{\epsilon_{BLG}} - \frac{n^*e^2d}{\epsilon_{BLG}} \tag{30}$$

where net charge density is

$$n^* = \frac{N_c\delta}{\gamma_1}\ln\left(\frac{\gamma_1}{\delta} + \sqrt{1+(\frac{\gamma_1}{\delta})^2}\right) \tag{31}$$

The interlayer asymmetry 2δ is then invariably *less* than it would be in the case where the layers are not charged, leading us to refer to this as a screening effect. Finally, this effective two band tight binding model leads to a self consistency equation, from which we can get quantitatively bandgap with variable external displacement field,

$$2\delta + \frac{N_c\delta}{\gamma_1}\ln\left(\frac{\gamma_1}{\delta} + \sqrt{1+(\frac{\gamma_1}{\delta})^2}\right)\frac{e^2d}{\epsilon_{BLG}} = \frac{D_{ext}ed}{\epsilon_{BLG}} \tag{32}$$

We can finally calculate the bandgap in the regime of the two band effective Hamiltonian,

$$\Delta = 2\delta \tag{33}$$

As Fig. 10 shows, a tunable bandgap as large as 250meV has been achieved in previous experiments [13]. For comparison, we have used three different methods of theoretical computation to generate the bandgap Δ as a function of D_{ext}, plotted in Fig. 10. Compared with the unscreened result, the self-consistent screening method fits very well to experiments in the low field regime. In the intermediate and high field regime, the dispersion relation is not accurate any more because we expect the bandgap to begin to saturate as it approaches γ_1. This is perfectly intuitive - as we begin to pull electrons from one layer to the other that are far from the K points, our two band approximation should fall apart. What is happening mathematically is that we assumed a maximum electron density $5\times10^{12}cm^{-2}$, much smaller than the typical values on the order of $10^{19}cm^{-2}$ in real bilayer graphene. Full range fitting requires a self-consistent tight binding method based on the full, four band Hamiltonian.

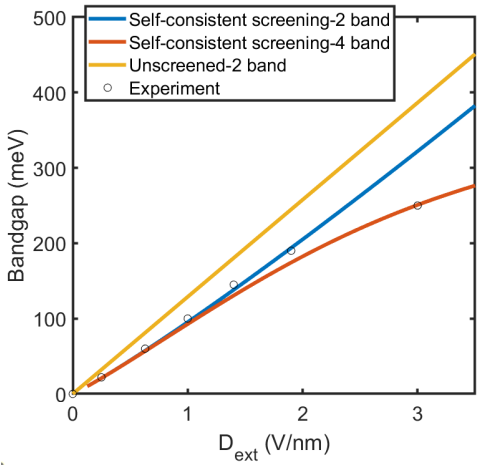

FIG. 10: Comparison of our theoretical calculations in the two band and four band regimes with experimental results. Experimental results from [13] are plotted in circles. The blue line represents the results produced in our analysis in the preceding section, using a screening function and bandgap consistent with the two band effective Hamiltonian. The red line represents the result when we use the screening function calculated for the two band Hamiltonian, and a bandgap consistent with the four band Hamiltonian.

V. OPTICAL PROPERTIES OF BILAYER GRAPHENE

A. Pseudospin Texture

As we have already discussed in Sec.III.C, the eigenvectors for our effective two-band Hamiltonian are:

$$|c,k\rangle = \begin{pmatrix} \cos(\frac{\theta_k}{2}) \\ \sin(\frac{\theta_k}{2})e^{2i\phi_k} \end{pmatrix} \qquad |v,k\rangle = \begin{pmatrix} \sin(\frac{\theta_k}{2})e^{-2i\phi_k} \\ \cos(\frac{\theta_k}{2}) \end{pmatrix}$$

Under our low energy two-band approximation, the eigenstates in the conduction band and valence band state resemble the form of a spinor, which is pointing along $\vec{n} = (\sin(\theta)\cos(\phi), \sin(\theta)\sin(\phi), \cos(\theta))$. This is often called a *pseudospinor* - the difference between this *pseudospinor* and the spinors that we're familiar with (especially those of us currently in PHYS500) is that the angles determining the direction of the pseudospinor are in k-space rather than real space, and that there is a factor of two in the phase $e^{2i\phi_k}$. As shown in Fig. 11, when the parameter $\vec{k} = (k_x, k_y)$ rotates counter-clockwise around the K valley by an angle 2π, the pseudospin actually rotates by 4π in the same direction, giving a winding number $\omega = 2$, similar to orbital angular momentum. The concept of pseudospin is more than just a mathematical oddity, and has measurable physical consequences. The conduction and valence band pseudospinors are linear combinations of the two non-dimer site basis states. The pseudospin up state pointing out of the interlayer axis corresponds to electrons residing exclusively on site α_1, and similarly the pseudospin down state corresponds to electrons residing exclusively on site α_2. For zero interlayer asymmetry, the electrons are equally distributed on these two sites, making the pseudospin lie parallel with the graphene plane, rotating with $\vec{k} = (k_x, k_y)$.

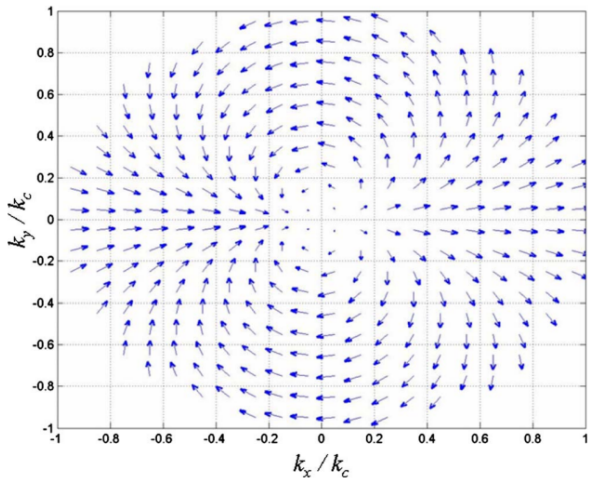

FIG. 11: Projection distribution in k_x and k_y plane. If the parameter (k_x, k_y) rotates about the origin by 1 cycle, the pseudospin rotates by 2 cycles corresponding to a winding number $\omega = 2$ [15].

So far, all calculations have been performed near the K valley - for the $K^{'}$ valley, the pseudospin winding number is $\omega - 2$, meaning (in a semiclassical sense) that the pseudospin rotates in a direction opposite to that of the K valley. This indicates the presence of some kind of *chiral* fermions in bilayer graphene.

B. Excitonic states in biased bilayer graphene

Excitons are composed of an electron-hole pair bound through the Coulomb attraction, and are widely understood in conventional semiconductors such as GaAs. The widely (several hundred meV) electrically tunable bandgap in bilayer graphene opens a new opportunity to study excitonic states in this system. In recent years, excitons in biased bilayer graphene have been observed via Fourier transform spectroscopy. [16].

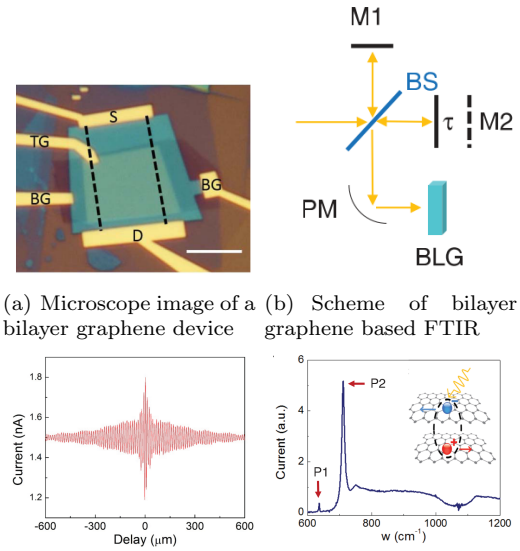

(a) Microscope image of a bilayer graphene device

(b) Scheme of bilayer graphene based FTIR

(c) A typical FTIR measurement result

(d) Absorption spectrum of bilayer graphene

FIG. 12: Observation of a p-state exciton in biased bilayer graphene, giving strong evidence for a pseudospin winding effect[16].

As shown in Fig. 12(a), a piece of bilayer graphene is encapsulated by two layers of h-BN with two electrodes (source and drain) measuring a photo-current. The back gate can be used to tune free carrier densities while the top gate applies a vertical electric field to open a bandgap in near infrared to mid infrared frequencies. An FTIR spectrum is used to measure bilayer absorption as shown in Fig. 12(b). After propagating through the Michelson interferometer with delay τ, the light is incident on the graphene sample with an intensity:

$$I(\tau) = \xi_1^2 + \xi_2^2 + \xi_1\xi_2(e^{-2ik_\lambda c\tau} + e^{2ik_\lambda c\tau}) \qquad (34)$$

As you can see, there are two D.C. terms, as well as a term oscillating with frequency $2k_\lambda$. There will be a strong photo-current detected if bilayer graphene absorbs at a wavelength that will generate electron-hole pairs, due to the biased voltage between source and drain dissociating excitons into free carriers. The photo-current will be proportional the absorption coefficient, resulting in the equation:

$$j(\tau) = \int [\xi_1^2(k_\lambda) + \xi_2^2(k_\lambda) + \xi_1(k_\lambda)\xi_2(k_\lambda)(e^{-2ik_\lambda c\tau} + e^{2ik_\lambda c\tau})]\alpha(k_\lambda)dk_\lambda \tag{35}$$

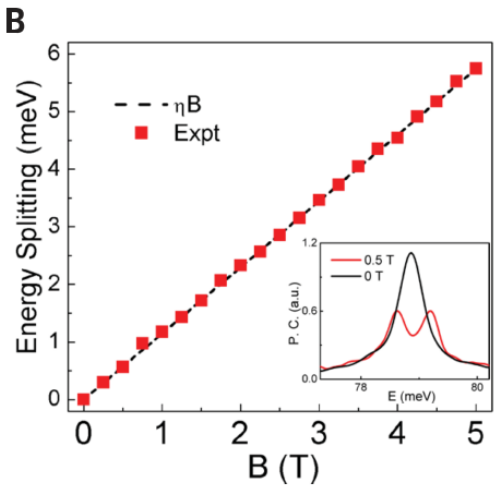

FIG. 13: Zeeman effect of excitonic peak[16]

In experiments, one can make $\epsilon_1(k_\lambda)$ and $\epsilon_2(k_\lambda)$ nearly independent of k_λ with the right choice of light source and mirrors, which means that the absorption coefficient for the sample at a given wavelength will be recorded as the Fourier component for frequency k_λ. The absorption spectrum can then be constructed simply by Fourier transforming the so-called "interferogram" collected by measuring the photocurrent. As shown in Fig. 12(c) and 12(d), the absorption spectrum of bilayer graphene shows two excitonic peaks within the bandgap.

Surprisingly, bilayer graphene's absorption spectrum indicates that absorption lines for p-like excitons (with $\ell = 1$) are very intense, while in conventional quantum wells like GaAs, the selection rule forbidding these p-like transitions is very strict. Although a quantitative description of this drastic difference requires a deeper analysis than we can justify including in this paper, we can still develop a qualitative understanding of this phenomenon based on the effective two band model and our understanding of pseudospin texture developed in the previous section.

It turns out the winding pseudospin is equivalent to an internal orbital moment along z direction, corresponding to a magnetic momentum ± 2. In the formation of electron-hole pairs, angular momentum must be conserved, so the sum of the electrons internal angular momentum and the angular momentum of the photon is equal to the angular momentum of the exciton envelope wave function.[16]

$$m_{env} = m_{pseudospin} + m_{photon} \tag{36}$$

For the K valley we have $m_{pseudospin} = +2$, which can couple with left handed photons with $m_{photon} = -1$, making the creation of a p-state exciton optically allowed. This has been verified both experimentally, and with much more theoretical rigor in [17].

In the presence of a magnetic field, this transition splits into two Zeeman components as shown in Fig. 13. This confirms that the excitation is p-like, and that the internal magnetic moment must be contributed by pseudospin- the conduction band and valence band are both composed of p_z orbitals with zero angular momentum projection on the z axis, and electron and hole pairs have opposite spin. We also observe in these experiments that the s-type exciton transitions are not strictly forbidden - this can be shown to be a consequence of the trigonal warping term.[16]

VI. LANDAU LEVELS IN BILAYER GRAPHENE

In this section, we will briefly discuss solutions of the electronic Hamiltonian in bilayer graphene under a strong magnetic field. In a conventional 2D electron gas system, the conductivity tensor component σ_{xy} perpendicular to the in-plane electric field shows a step function like dependence on a strong out of plane magnetic field, a phenomenon known as the integer quantum Hall effect. The step space is precisely $2e^2/h$ - for a detailed analysis of the integer quantum hall effect, see Philipp, Simon, Jun, and Aly's project from last year - we found it very helpful. The integer quantum hall effect has been observed in monolayer and bilayer graphene. [18]. Based on the two band effective Hamiltonian of bilayer graphene in the low energy approximation Eq.19, electrons in a magnetic field $B\hat{z}$ are described by a Hamiltonian:

$$H = \frac{1}{2m}\begin{pmatrix} 0 & P_-^2 \\ P_+^2 & 0 \end{pmatrix} \tag{37}$$

where $P_+ = \hbar k_x + i\hbar k_y - ieBx = P_-^\dagger$ when we choose the Landau gauge with vector potential $A = (0, -Bx, 0)$. The commutator relation between P_+ and P_- is:

$$[P_-, P_+] = -2\hbar eB \tag{38}$$

In this case, the energy spectrum is given by,

$$\begin{aligned} E^2 =& \frac{1}{4m^2} P_- P_- P_+ P_+ \\ =& \left(\frac{P_- P_+}{2m}\right)^2 - \hbar\omega_B \frac{P_- P_+}{2m} \end{aligned} \tag{39}$$

where $\omega_B = \frac{\hbar eB}{m}$; the energy spectrum of $\frac{P_- P_+}{2m}$ is:

$$\frac{P_- P_+}{2m} = \frac{\hbar^2 k_x^2}{2m} + \frac{(\hbar k_y + eBx)^2}{2m} - \frac{1}{2}\hbar\omega_B = l\hbar\omega_B \quad (40)$$
$$l = 0, 1, 2, 3...$$

When we substitute Eq. 40 into the eigen-equation for the bilayer spectrum, we obtain:

$$E_{l,\pm} = \pm\hbar\omega_B\sqrt{l(l-1)}, \quad (41)$$

We notice that there are two main differences compared with conventional Landau levels in a 2D electron gas. First, in the bilayer system, there are energy bands corresponding to both an electron gas and a hole gas. Secondly, the ground state is doubly degenerate in orbital angular momentum, having the same energy for $l = 1$ and $l = 0$. After considering spin and valley degeneracy, the total degeneracy factor for the ground state is $g = 8$. This results in an unusual quantum Hall effect in bilayer graphene, with an unconventionally large step in the conductance at zero carrier density, as shown in Fig. 14.

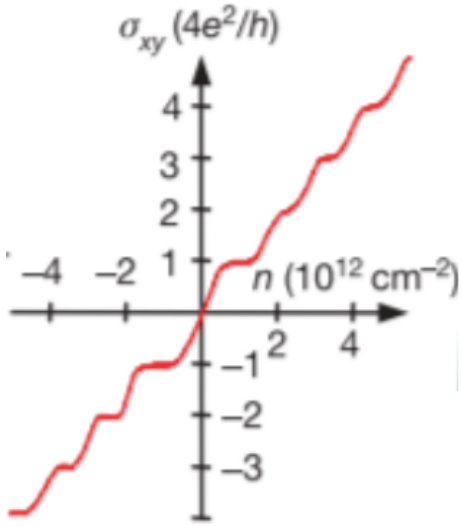

FIG. 14: Quantum Hall effect in bilayer graphene. Step spacing at zero density is $\Delta\sigma = 8e^2/h$ [19].

VII. CONCLUSION

The study of bilayer graphene systems has been a frontier in condensed matter physics for nearly two decades. One of the most valuable and important properties of graphene is the electrically tunable bandgap we introduced in this paper - a semiconductor with a tunable bandgap could have powerful and far-reaching implications in electronics. New degrees of freedoms such as valley and pseudospin cause a broad range of emergent phenomena in this system, and are exciting potential new avenues for storing and manipulating information in quantum systems. What is most fascinating is that our relatively simple theoretical analysis based on the tight binding model provides a very accurate description of the electronic behavior of graphene in electric and magnetic fields, due mainly to electrons in the graphene system generally having weak correlations, making the non-interacting Hamiltonian a very good approximation in all but the most obscure cases.

Graphene still has many secrets to hide, however - recently, the study of graphene has been pushed into a new era after the recent observation of unconventional superconductivity in twisted bilayer graphene in 2018. [20] Condensed matter physicists are hopeful that if the mechanism leading to superconductivity in graphene could be understood, it would lead to us having a better understanding of unconventional superconductivity in other materials, potentially leading to a revolution in modern technology.

Appendix A: Effective two band Hamiltonian[8]

The effective four band Hamiltonian around K point can be rewritten as

$$H_{eb} = \begin{pmatrix} H_{11} & H_{12} \\ H_{21} & H_{22} \end{pmatrix} \quad (A1)$$

In the basis $(\alpha_1, \beta_2, \alpha_2, \beta_1)^T$, the four 2×2 blocks are:

$$H_{11} = \begin{pmatrix} -\delta & 0 \\ 0 & -\delta \end{pmatrix} \qquad H_{12} = \begin{pmatrix} 0 & v_0\pi^\dagger \\ v_0\pi & 0 \end{pmatrix}$$

$$H_{21} = \begin{pmatrix} 0 & v_0\pi \\ v_0\pi^\dagger & 0 \end{pmatrix} \qquad H_{22} = \begin{pmatrix} -\delta & \gamma_1 \\ \gamma_1 & \delta \end{pmatrix}$$

We assume $l = (\alpha_1, \beta_2)^T$ corresponds to the inner bands while $h = (\alpha_2, \beta_1)^T$ represents the outer bands. The stationary Schrodinger equation is now reduced to

$$\begin{pmatrix} H_{11} & H_{12} \\ H_{21} & H_{22} \end{pmatrix} \begin{pmatrix} l \\ h \end{pmatrix} = E \begin{pmatrix} l \\ h \end{pmatrix} \quad (A2)$$

We can write this as a system of linear equations for h and l

$$h = (E - H_{22})^{-1} H_{21} l \quad (A3)$$

$$(H_{11} + H_{12}(E - H_{22})^{-1} H_{21}) l = El \quad (A4)$$

It should be pointed out that effective two band Hamiltonian approximation is only justified in the low energy regime, $\gamma_1 \gg E$. So that compared with H_{22} , the eigenvalue can be omitted on the right side of equation (A4)

. The final form of the effective two band Hamiltonian is:

$$H_{eff} = H_{11} - H_{12}H_{22}^{-1}H_{21} \tag{A5}$$

Appendix B: MATLAB Source Code - Diagonalizing Full Hamiltonian

```
%Appendix B - bilayerg.m
%Bradley Guislain
%Numerically diagonalizes tight-binding
%Hamiltonian for bilayer graphene.

clc;
clear;

%Construct k-space grid
kx = [-2.1*pi/(3):0.01:2.1*pi/(3)];
ky = [-2.1*pi/sqrt(3):0.01:2.1*pi/sqrt(3)];

%Define hopping parameters
t0 = 1;
t1 = 0.8;
t3 = 0.2;
t4 = 0.2;

%Interlayer asymmetry
U = 0;

%Realistic parameters
%t1 = 0.381/3.16;
%t3 = 0.38/3.16;
%t4 = 0.14/3.16;


%Diagonalizing:
for n = 1:length(kx)
for m = 1:length(ky)

    f(n,m) = exp(-i*kx(n)) + ...
    2*cos(sqrt(3)*0.5*ky(m))*exp(0.5*i*kx(n)/2);

    u = f(n,m);
    v = conj(f(n,m));

    H{n,m} = [U,-t0*u,t4*u,t3*v;...
    -t0*v,U,t1,t4*u;...
    t4*v,t1,-U,-t0*u;...
    t3*u,t4*v,-t0*v,-U];

    E{n,m} = eig(H{n,m});
    Emat = E{n,m};

    for k = 1:4
        bands{k}(n,m) = Emat(k);
    end
end
end

%Plotting:
figure(1)
hold on
for k = 1:4
    band = bands{k};
    surf(ky,kx,band)
    shading interp
    colormap jet
end
xlabel('k_ya')
ylabel('k_xa')
zlabel('E/\gamma_0')

%------------------
```


[1] S. Reich, J. Maultzsch, C. Thomsen, and P. Ordejón, Tight-binding description of graphene, Phys. Rev. B **66**, 035412 (2002).

[2] H. B. Nielsen and M. Ninomiya, The adler-bell-jackiw anomaly and weyl fermions in a crystal, Physics Letters B **130**, 389 (1983).

[3] A. Bostwick, J. McChesney, T. Ohta, E. Rotenberg, T. Seyller, and K. Horn, Experimental studies of the electronic structure of graphene, Progress in Surface Science **84**, 380 (2009).

[4] E. Mostaani, N. Drummond, and V. Fal'Ko, Quantum monte carlo calculation of the binding energy of bilayer graphene, Physical Review Letters **115**, 115501 (2015).

[5] L. Malard, J. Nilsson, D. Elias, J. Brant, F. Plentz, E. Alves, A. C. Neto, and M. Pimenta, Probing the electronic structure of bilayer graphene by raman scattering, Physical Review B **76**, 201401 (2007).

[6] X. Zhang, W.-Y. Shan, and D. Xiao, Optical selection rule of excitons in gapped chiral fermion systems, Physical review letters **120**, 077401 (2018).

[7] E. McCann and V. I. Fal'ko, Landau-level degeneracy and quantum hall effect in a graphite bilayer, Physical review letters **96**, 086805 (2006).

[8] E. McCann, Asymmetry gap in the electronic band structure of bilayer graphene, Physical Review B **74**, 161403 (2006).

[9] T. Ohta, A. Bostwick, T. Seyller, K. Horn, and E. Rotenberg, Controlling the electronic structure of bilayer graphene, Science **313**, 951 (2006).

[10] S. Y. Zhou, G.-H. Gweon, A. Fedorov, d. First, PN, W. De Heer, D.-H. Lee, F. Guinea, A. C. Neto, and A. Lanzara, Substrate-induced bandgap opening in epitaxial graphene, Nature materials **6**, 770 (2007).

[11] A. Kuzmenko, E. Van Heumen, D. Van Der Marel, P. Lerch, P. Blake, K. Novoselov, and A. Geim, Infrared spectroscopy of electronic bands in bilayer graphene,

Physical Review B **79**, 115441 (2009).
[12] Z. Li, E. Henriksen, Z. Jiang, Z. Hao, M. C. Martin, P. Kim, H. Stormer, and D. N. Basov, Band structure asymmetry of bilayer graphene revealed by infrared spectroscopy, Physical Review Letters **102**, 037403 (2009).
[13] Y. Zhang, T.-T. Tang, C. Girit, Z. Hao, M. C. Martin, A. Zettl, M. F. Crommie, Y. R. Shen, and F. Wang, Direct observation of a widely tunable bandgap in bilayer graphene, Nature **459**, 820 (2009).
[14] H. Min, B. Sahu, S. K. Banerjee, and A. MacDonald, Ab initio theory of gate induced gaps in graphene bilayers, Physical Review B **75**, 155115 (2007).
[15] H. Min, G. Borghi, M. Polini, and A. H. MacDonald, Pseudospin magnetism in graphene, Physical Review B **77**, 041407 (2008).
[16] L. Ju, L. Wang, T. Cao, T. Taniguchi, K. Watanabe, S. G. Louie, F. Rana, J. Park, J. Hone, F. Wang, *et al.*, Tunable excitons in bilayer graphene, Science **358**, 907 (2017).
[17] T. Cao, M. Wu, and S. G. Louie, Unifying optical selection rules for excitons in two dimensions: Band topology and winding numbers, Physical review letters **120**, 087402 (2018).
[18] L. Landau, Diamagnetismus der metalle, Zeitschrift für Physik **64**, 629 (1930).
[19] K. S. Novoselov, A. K. Geim, S. Morozov, D. Jiang, M. I. Katsnelson, I. Grigorieva, S. Dubonos, Firsov, and AA, Two-dimensional gas of massless dirac fermions in graphene, nature **438**, 197 (2005).
[20] Y. Cao, V. Fatemi, S. Fang, K. Watanabe, T. Taniguchi, E. Kaxiras, and P. Jarillo-Herrero, Unconventional superconductivity in magic-angle graphene superlattices, Nature **556**, 43 (2018).